



Carbon dioxide Fischer-Tropsch synthesis: A new path to carbon-neutral fuels



Yo Han Choi^{a,1}, Youn Jeong Jang^{b,1}, Hunmin Park^b, Won Young Kim^b, Young Hye Lee^b, Sun Hee Choi^c, Jae Sung Lee^{d,*}

^a Division of Advanced Nuclear Engineering, Pohang University of Science and Technology(POSTECH), Pohang 790-784, South Korea

^b Department of Chemical Engineering, Pohang University of Science and Technology(POSTECH), Pohang 790-784, South Korea

^c Pohang Accelerator Laboratory, Pohang University of Science and Technology(POSTECH), Pohang 790-784, South Korea

^d School of Energy and Chemical Engineering, Ulsan National Institute of Science and Technology (UNIST), Ulsan 689-798, South Korea

ARTICLE INFO

Article history:

Received 20 July 2016

Received in revised form

21 September 2016

Accepted 28 September 2016

Available online 29 September 2016

Keywords:

Carbon capture and utilization

Carbon-neutral fuels

Copper-iron catalyst

Liquid hydrocarbons

CO₂ Fischer-Tropsch synthesis

ABSTRACT

Paradigm of climate change mitigation technologies is shifting from carbon capture and storage (CCS) to carbon capture and utilization (CCU). Here we propose a new path to CCU – direct CO₂ conversion to liquid transportation fuels by reacting with renewable hydrogen produced by solar water splitting. The highly promising and CO₂-neutral CCU system is possible by our discovery of a new catalyst that produces liquid hydrocarbon (C₅₊) selectivity of ~65% and greatly suppressed CH₄ formation to 2–3%, which represents an unprecedented selectivity pattern for direct catalytic CO₂ hydrogenation and is very similar to that of conventional CO-based Fischer-Tropsch (FT) synthesis. The catalyst was prepared by reduction of delafossite-CuFeO₂ and *in-situ* carburization to Hägg carbide (χ -Fe₅C₂), the active phase for heavy hydrocarbon formation. The reference catalysts derived from bare Fe₂O₃, CuO-Fe₂O₃ mixture, and spinel CuFe₂O₄ are much less active and produce mainly light hydrocarbons, highlighting the critical role of delafossite-CuFeO₂ as the catalyst precursor. The new catalyst breaks through the limitation of CO₂-based FT synthesis and will open the avenue for new opportunity for carbon recycling into valuable liquid fuels at the similar conditions to industrially practiced CO-FT synthesis.

© 2016 Elsevier B.V. All rights reserved.

1. Introduction

An unrelenting growth of CO₂ emission into the atmosphere threatens the world's sustainability with the global warming. Carbon capture and storage (CCS) has been considered as the most effective technology of mitigation options. Yet, the past years have observed that storage of CO₂ in a geological reservoir has significant drawbacks of the possible leakage, long-term liability, and availability of enough storage capacity in many regions of the world. Naturally, global interest has been shifting from CCS to carbon capture and utilization (CCU) that converts the captured CO₂ into useful products such as fuels, chemicals, plastics, and alternative building materials [1]. Among proposed options of CCU, conversion of CO₂ into hydrocarbon fuels compatible with our current storage and distribution network is most attractive. It represents a CO₂-neutral path because the fuels turn to CO₂ again upon com-

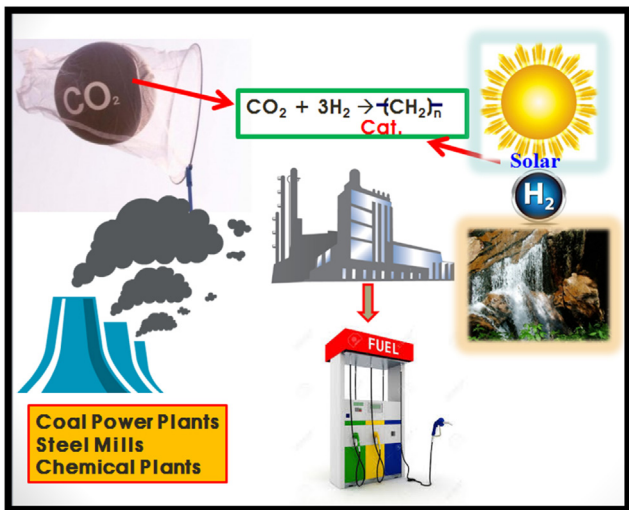
bustion. Yet, to the extent that the carbon-neutral fuels replace fossil fuels, they result in negative CO₂ emission or net CO₂ removal from the atmosphere. Making hydrocarbons out of CO₂ must overcome two challenges – chemical stability of the CO₂ molecule and a cheap and renewable hydrogen source. Catalytic hydrogenation of CO₂ has been studied intensively, but the products of direct hydrogenation are limited mostly to low molecular weight (C₁–C₄) hydrocarbons or oxygenates (CO, CH₃OH, HCOOH, CH₃OCH₃, etc.) instead of heavier liquid hydrocarbons more suitable for transportation fuels [2–10].

Here we propose a new path to CCU – direct CO₂ conversion to liquid fuels with renewable hydrogen produced by solar water splitting as depicted in Scheme 1. Thus, CO₂ emitted from industrial sources like coal power plants, steel mills, or chemical plants is captured and reacts with H₂ generated from solar hydrogen plant to produce liquid fuels in a single step. Our direct CO₂-FT synthesis is different from the CO₂-to-diesel conversion process recently announced by Audi, which actually involves two steps – reverse water gas shift (RWGS) reaction to CO followed by CO Fisher-Tropsch (FT) synthesis [11]. The solar water splitting to produce hydrogen is developing rapidly lately and highly efficient

* Corresponding author.

E-mail address: jlee1234@unist.ac.kr (J.S. Lee).

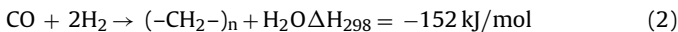
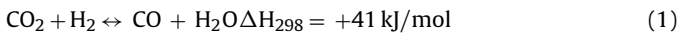
¹ These authors contributed equally to this work.



Scheme 1. Proposed carbon capture and utilization (CCU) system based on catalytic CO₂ conversion to liquid hydrocarbon fuels with hydrogen supplied from solar water splitting.

PV-electrolysis [12] or photoelectrochemical systems [13,14] have been developed. Hence, this report focusses on the catalytic CO₂-to-liquid fuel conversion (CO₂ FT synthesis) with renewable H₂.

Hydrogenation of CO₂ to hydrocarbons consists of two reactions in series – RWGS reaction (Eq. (1)) and FT synthesis (Eq. (2)) [15].



Compared to conventional CO-FT reaction with synthesis gas (a mixture of CO and H₂), CO₂ hydrogenation involves three moles of hydrogen per mole of CO₂ and produces plenty of byproduct water, which is a deactivation agent for iron-based FT catalysts. Hence, CO₂ hydrogenation is much slower than CO-FT reaction under the same conditions [15]. The hydrocarbon products include light hydrocarbons (C₁-C₄ paraffins and olefins), and heavier hydrocarbons (C₅⁺), and oxygenates [16]. Because CO is the chain growing agent in FT reaction, CO₂ hydrogenation produces mainly low molecular weight hydrocarbons instead of C₅⁺ products that are more valuable as liquid transportation fuels.

The CO₂ hydrogenation to hydrocarbons has been studied mainly on traditional catalysts for CO-FT synthesis and Fe-based catalysts are favored over Co, Ni and Ru because of their RWGS activity and relatively higher selectivity for C₂⁺ hydrocarbons. The selectivity of Fe catalysts for C₅⁺ products could be further improved by employing proper promoters. Widely studied promoters to tailor the product distribution of Fe catalysts include second metals (Mn, Cu, La, Zr, Cr, Mo, or Ta), alkaline metals (Na, K, or Rb), and metal oxides (α -Al₂O₃ and TiO₂) [7,17–23]. In spite of improvement by these promoters, the selectivity for C₅⁺ hydrocarbons is much lower than that obtained from CO-FT synthesis over similar catalysts.

Our novel Cu–Fe catalyst derived from delafossite-CuFeO₂ produces heavy hydrocarbons from CO₂ hydrogenation in the same manner as from conventional CO-FT synthesis. Thus, reduction and *in-situ* carburization CuFeO₂ formed effectively the Hägg iron carbide (χ -Fe₅C₂), the known active catalytic phase for the formation of heavier hydrocarbons in FT synthesis. The unique role of delafossite-CuFeO₂ as the catalyst precursor is evident because Cu–Fe reference catalysts derived from Cu₂O–Fe₂O₃ mixture and spinel CuFe₂O₄ were much less active and produced mainly light hydrocarbons highlighting the critical role of delafossite-CuFeO₂ as the catalyst precursor.

2. Experimental

2.1. Catalyst preparation

Delafossite-CuFeO₂ was prepared by a simple hydrothermal method according to a reported procedure [24–26]. Thus, 2.02 g of Fe(NO₃)₃·9H₂O and 1.2 g of Cu(NO₃)₂·3H₂O were dissolved in 40 ml of distilled water and then 0.1 mol NaOH was added into the solution to maintain the basic condition. After stirring for 30 min, 0.5 ml of propionaldehyde was added as reduction agent for copper (II) to copper (I). The mixture was transferred to 100 ml Teflon-lined stainless steel autoclave and hydrothermal reaction took place at 180 °C for 6–24 h. The synthesized products are designated as CuFeO₂-6, CuFeO₂-12, and CuFeO₂-24 depending on the synthesis time of 6, 12 and 24 h, respectively. Spinel CuFe₂O₄ nanopowders (<100 nm) was purchased from Sigma-Aldrich and bare Fe₂O₃ from Kanto, and used as received. All the prepared catalysts are denoted by their precursors, *i.e.* ex-CuFeO₂, ex-CuFe₂O₄, and ex-Fe₂O₃

2.2. Catalytic CO₂ hydrogenation

The catalytic CO₂ hydrogenation was carried out in a fixed bed, stainless steel reactor with a CO₂/H₂ ratio of 1:3. The pre-reduction was performed under 100 sccm of pure H₂ at 400 °C for 2 h. For catalytic reaction, CO₂ and H₂ were supplied into reactor with N₂ as an internal standard gas to calculate CO₂ conversion. The reaction conditions were 300 °C, 10 bar and a gas hourly space velocity (GHSV) of 1800 ml g⁻¹ h⁻¹. Concentrations of the CO₂, CO products and N₂ were measured by an on-lined Agilent 7890A gas chromatograph with a thermal conductivity detector and a Carboxen 1000 packed column. Hydrocarbons of C₁-C₆ were analyzed with the same GC with a flame ionization detector and an Alumina Sulfate PLOT Capillary column. The heavier hydrocarbon products were collected in cold trap. The composition of the heavy hydrocarbons was calculated on weight percent of carbon number by using simulated distillation (SIMDIS) analysis.

2.3. Characterization and product analysis

High-resolution transmission electron microscopy (HR-TEM) and scanning electron microscopy (SEM) were carried out on JEOL JEM-2200FS and Philips Electron Optics B. V. XL30S FEG, operated at 10 keV. Powder X-ray diffraction (XRD) patterns were collected from PANalytical x'pert using Cu K α radiation. Temperature-programmed reduction (H₂-TPR) was performed on an AutoChem II apparatus of Micromeritics. Pore size distribution and BET surface area were analyzed by N₂ sorption isotherms measured at 77 K on Mirae SI, Nanoporosity-XQ apparatus. X-ray photoelectron spectroscopy (XPS) was carried out on ESCALAB 250xi using Al K α radiation.

X-ray absorption fine structure (XAFS) experiments were carried out on 7D beamline of Pohang Accelerator Laboratory (PLS-II, 3.0 GeV, 400 mA). The synchrotron radiation was monochromatized using a Si(111) double crystal monochromators. At room temperature, spectra for the Fe K-edge ($E_0 = 7112$ eV) and the Cu K-edge ($E_0 = 8979$ eV) were taken in a transmission mode. The incident beam was detuned by 30% for the Fe K-edge and by 20% for the Cu K-edge in order to minimize contamination of higher harmonics and its intensity was monitored using He-filled and N₂-filled IC SPEC ionization chambers for Fe and Cu K-edges, respectively. For each sample, a reference spectrum of Fe foil or Cu foil was recorded simultaneously so that the energy in the spectrum of sample could be calibrated with respect to the K-edge energy of Fe metal or Cu metal. The AHENA in the IFEFFIT suite of programs was used to ana-

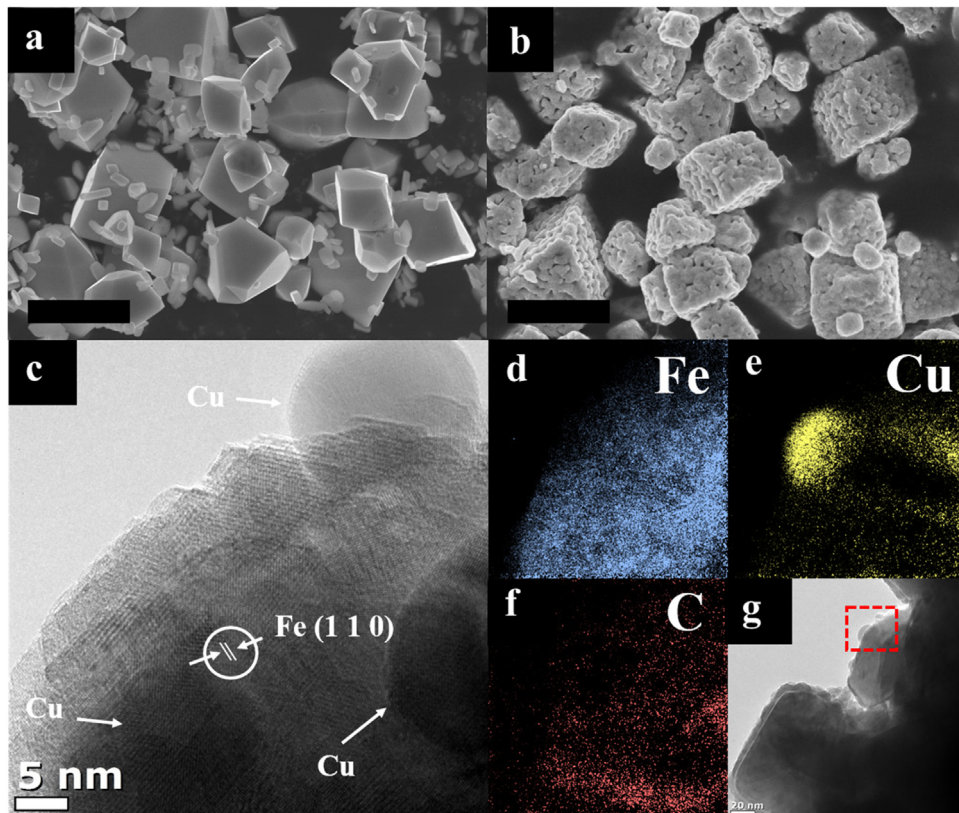


Fig. 1. SEM images of rhombohedral CuFeO_2 crystals synthesized by hydrothermal reaction for 12 h (a) and $\text{CuFeO}_2\text{-}12$ reduced by H_2 (b) (scale bar, 2.5 μm). HR-TEM images of reduced $\text{CuFeO}_2\text{-}12$ (c), and EELS mapping images of Fe (d), Cu (e) and C (f) for indicated area in the image in (g) of the used $\text{CuFeO}_2\text{-}12$.

lyze the obtained data to determine the local structures of Fe and Cu in CuFeO_2 , CuFe_2O_4 and Fe_2O_3 catalysts.

3. Results

3.1. Physicochemical properties of the catalysts

As described in Experimental, delafossite- CuFeO_2 was synthesized by a hydrothermal method according to a reported procedure [24–26]. The catalyst precursor has delafossite CuFeO_2 structure as shown by the XRD pattern (JCPDS card 01-075-2146) in Fig. S1 of Supporting information (SI). The impurity phases of Fe_2O_3 and Cu_2O are also observed with main diffraction peaks at $2\theta = 33$ and 38.9° , respectively, but their intensity gets diminished as the hydrothermal time increases from 6 to 24 h. All the CuFeO_2 samples reduced at 400°C for 2 h exhibit two intense diffraction peaks at 43.3 and 44.7° identified as Cu and Fe metals, respectively (Fig. S1b). The same metallic phases are also observed for reduced CuFe_2O_4 of the original inverse spinel structure, but Fe in this reference catalyst has a higher intensity. Thus both CuFeO_2 and CuFe_2O_4 form separate phases of metallic Cu and Fe upon reduction.

Morphological details of synthesized catalysts were analyzed by scanning and transmission electron microscopy (SEM, TEM). As shown in Figs. 1 and S2, CuFeO_2 forms rhombohedral crystals of $\sim 1.0 \mu\text{m}$ together with many smaller particles of Cu_2O and Fe_2O_3 impurities that join into CuFeO_2 crystals with extended hydrothermal reaction following an Ostwald ripening process. This hydrothermal method allows easy synthesis of crystalline CuFeO_2 at a low temperature compared to other synthesis methods [27,28]. Upon reduction, many macropores are developed in CuFeO_2 particles with the original rhombohedral morphology and size preserved (Fig. 1b). The evolution of textural properties

extracted from N_2 adsorption-desorption isotherms is presented in Figs. S3–S4 and Table S1 of SI. The reference spinel CuFe_2O_4 (Sigma-Aldrich) is made of small nanoparticles of 30–50 nm (Fig. S5). Fig. 1c exhibits HR-TEM images of reduced CuFeO_2 with H_2 , where spherical copper particles of $\sim 20 \text{ nm}$ in diameter are formed in contact with iron particles of irregular shape. Electron energy loss spectroscopy (EELS) mapping of CuFeO_2 -derived catalyst after the CO_2 hydrogenation at 300°C for 16 h in Fig. 1d–f indicates that carbon is well dispersed overlapping with the distribution of Fe, but no correspondence with Cu distribution. This could be taken as an initial sign of the iron carbide formation in CuFeO_2 -derived catalyst as discussed below.

3.2. Catalytic $\text{CO}_2 + \text{H}_2$ reactions

The prepared catalysts were investigated for $\text{CO}_2 + \text{H}_2$ reactions in a fixed bed, stainless steel reactor at 300°C , 10 bar with $\text{H}_2/\text{CO}_2 = 3$ and a gas hourly space velocity (GHSV) of $1800 \text{ mg g}^{-1} \text{ h}^{-1}$. Three reference catalysts were tested derived from spinel- CuFe_2O_4 , Fe_2O_3 , and 1:1 physical mixture of Cu_2O - Fe_2O_3 . The time curves and product distributions are summarized in Fig. 2 and Table 1. The reaction rates are expressed in Fe time yield (FTY = mol of CO_2 converted per g of Fe in the catalyst per second). The FTY remains stable after an early induction period of ca. 2 h. The FTY values are lower than typical values of CO hydrogenation on Fe-based catalysts by a factor of ~ 10 [29]. Their performance is compared with reported values for CO_2 hydrogenation over iron-based catalysts in Table S2 of SI. FTY of ex- CuFeO_2 is at least 2 times higher than other unsupported reference catalysts studied here. All catalysts have similar CO selectivity around 30% by the RWGS reaction. It indicates that Fe metal has a similar RWGS activity with or without copper. The most remarkable observation in Table 1 is

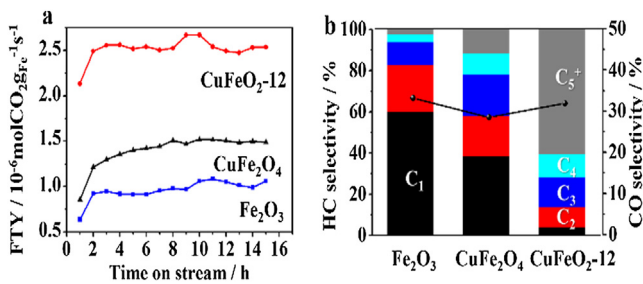


Fig. 2. (a) Fe time yield (FTY) against time on stream for catalysts derived from Fe_2O_3 , CuFe_2O_4 , and $\text{CuFeO}_2\text{-}12$ precursors. (Reaction conditions: 300°C , 10 bar, $1800 \text{ ml g}^{-1} \text{ h}^{-1}$, $\text{H}_2/\text{CO}_2 = 3$). (b) Product selectivity on CO-free basis.

that ex-CuFeO₂ catalyst exhibits extraordinary selectivity toward heavier hydrocarbons (C_5^+) and olefins. The C_5^+ selectivity higher than 65% is typically observed for CO-FT synthesis over iron-based catalysts, yet has never been reported so far in CO_2 hydrogenation as shown in Table S2. Equally impressive is the very low (2–3%) methane selectivity, which is also unusual in CO_2 hydrogenation. The ex-CuFeO₂ catalyst also shows a very high olefin-to-paraffin (O/P) ratio of 7.3 for $\text{C}_2\text{-}\text{C}_4$ hydrocarbons. Fig. S6 of SI represents the carbon number analysis using a simulated distillation method for liquid products collected from CO_2 hydrogenation over ex-CuFeO₂. The main products cover the gasoline ($\text{C}_5\text{-}\text{C}_{11}$) and diesel ($\text{C}_{12}\text{-}\text{C}_{21}$) ranges, while waxy hydrocarbons (C_{25}^+) are ~15 wt%. The product distribution is very similar to the one typically observed in CO-FT synthesis over iron catalysts [30].

The unique selectivity of ex-CuFeO₂ is evident in comparison with reference catalysts under the same conditions. First, the catalyst derived from Cu_2O (Alfa) did not show any CO_2 conversion at all indicating no activity for RWGS. Next, a physical mixture of $\text{Cu}_2\text{O}\text{-}\text{Fe}_2\text{O}_3$ (weight ratio = 1:1) manifests much lower CO_2 conversion, very little C_5^+ selectivity and small O/P ratio compared to ex-CuFeO₂. The product distribution is very similar to ex- Fe_2O_3 with no obvious beneficial effects of copper. Finally, the catalyst from spinel- CuFe_2O_4 with copper in the structure shows improved C_5^+ selectivity and O/P ratio, but only marginally. Alkali metals such as K and Na are usually introduced to iron catalysts in order to promote olefin selectivity in CO_2 hydrogenation. Our catalyst is unique in producing the high O/P ratio with no added alkali metal. The ICP analysis showed that ex-CuFeO₂ contained only 0.03% of Na residue from the preparation step, which is much lower than typical alkali-promoted iron catalysts. Thus there must be unique roles of delafossite CuFeO₂ as the catalyst precursor, not simply as a source of copper.

Additional kinetic studies were carried out for the ex-CuFeO₂ catalyst to find the effect of GHSV (Table S3) and CO/ CO_2 -cofeeding (Table S4). Pure CO hydrogenation shows a high CO conversion of 80.9% with increased FTY by a factor of 4.2. But the unique selectivity pattern (high C_5^+ selectivity, high O/P ration, and low methane

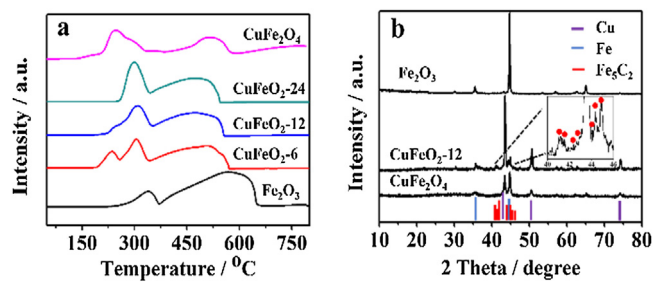


Fig. 3. (a) Temperature-programmed reduction (TPR) profile of various catalyst precursors. (b) XRD patterns after CO_2 hydrogenation at 300°C for 16 h. The bottom panel indicates expected peak positions for Cu, Fe, and Fe_5C_2 . Inset shows expanded pattern of ex-CuFeO₂-12 with $\chi\text{-Fe}_5\text{C}_2$ peaks highlighted.

selectivity) remain similar. The results confirm that our ex-CuFeO₂ catalyst shows very similar product distribution in the hydrogenation of both CO_2 and CO. Hence, our catalyst could be used as an efficient CO-FT synthesis catalyst as well. A longer term stability test in Fig. S7 indicates that the CO_2 conversion and C_5^+ selectivity remains invariant for 100 h on stream.

3.3. Unique role of delafossite- CuFeO_2 as the catalyst precursor

In this work, a novel Cu–Fe catalyst derived from delafossite- CuFeO_2 produces heavy liquid hydrocarbons and olefins selectively from CO_2 hydrogenation just like CO-FT synthesis. This represents the first demonstration that liquid fuels and olefins of high value and large market could be obtained directly from CO_2 , the most troublesome greenhouse gas. In addition to the practical significance, it is fundamentally interesting that Cu–Fe catalysts derived from $\text{Cu}_2\text{O}\text{-}\text{Fe}_2\text{O}_3$ mixture and spinel CuFe_2O_4 are much less active and produce mainly light paraffins, in spite of the similar Cu–Fe–O compositions in the form of a physical mixture as well as the crystal structure. Thus the unique product distributions could be obtained only when delafossite- CuFeO_2 is used as the catalyst precursor. A small amount of copper metal (typical molar ratio of Cu/Fe = 0.03–0.07) has long been used as a promoter for iron catalysts in CO-FT synthesis, where it serves as a reduction promoter facilitating the reduction of Fe^{3+} as well as carburization of Fe by CO/H_2 during the pretreatment or catalytic reaction. It is also reported that copper affects the performance of iron-based catalyst during the FT reaction as a separate metallic phase [31] or Cu^+ phase [32]. But any of the previous works cannot explain the dramatic precursor effect observed in this work.

In order to clarify the role of copper, the reducibility of the precursors was studied with temperature-programmed reduction ($\text{H}_2\text{-TPR}$) analysis in Fig. 3a. The TPR pattern of bare Fe_2O_3 catalyst shows the peaks at 340 and 560 °C, similar to the reported results [33]. All CuFeO₂ catalysts have distinctly lower reduction temperatures, indicating that copper promotes the reduction of

Table 1

CO_2 conversion and selectivity for catalysts derived from various precursors^a.

Catalyst	CO_2 Conv. [%]	CO sel. [%]	CO-free HC sel. [%]					O/P ^c
			C ₁	C ₂	C ₃	C ₄	C ₅ ⁺	
Fe_2O_3	14.3	33.2	60.2	22.5	11.3	3.7	2.3	0.03
CuFeO ₂ -6	17.3	31.7	2.7	8.3	12.6	10.1	66.3	7.3
CuFeO ₂ -12	18.1	31.9	3.9	10	14.5	11.3	60.3	7.0
CuFeO ₂ -24	16.7	31.4	2.4	8.7	13.3	10.7	64.9	7.7
CuFe_2O_4	13.3	28.4	38.3	19.7	20.1	10.5	11.4	0.02
$\text{Cu}_2\text{O}\text{-}\text{Fe}_2\text{O}_3$ ^b	15.7	28.9	57.6	22.8	12.6	4.4	2.6	0.03

^a Selectivity was calculated on CO-free basis.

^b Physically mixed Cu_2O and Fe_2O_3 (weight ratio = 1:1).

^c Olefins/paraffins ratio of $\text{C}_2\text{-}\text{C}_4$ products.

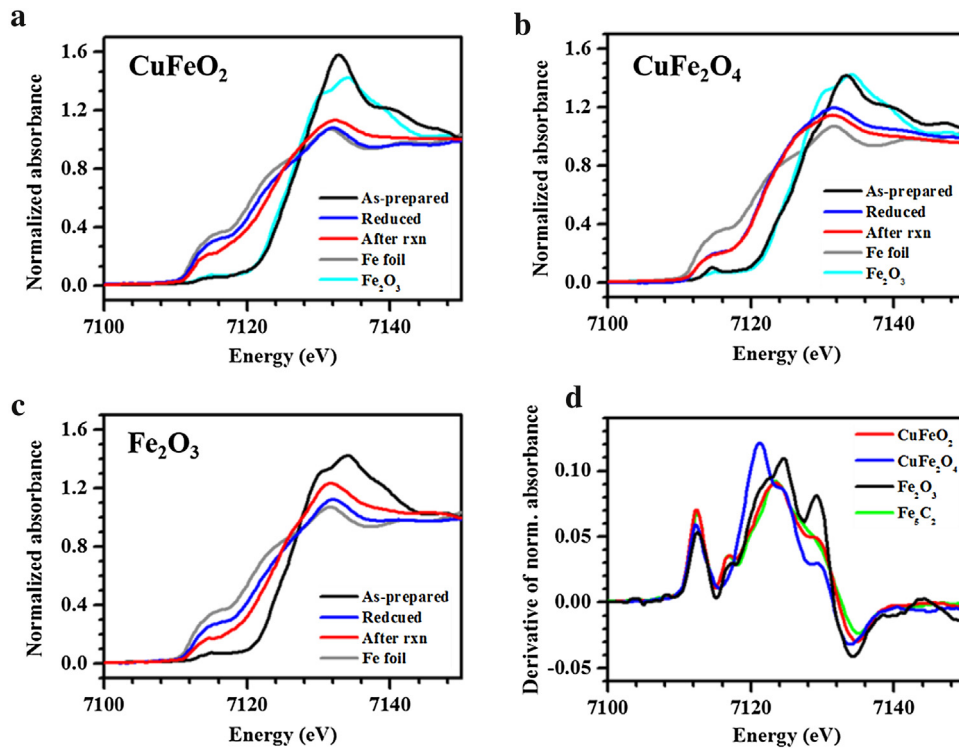


Fig. 4. Fe K-edge XANES spectra (a-c) and derivative spectra of normalized absorption (d) of iron-based catalysts: (a) CuFeO₂, (b) CuFe₂O₄, (c) Fe₂O₃, (d) after reaction for 16 h.

iron as reported. The shoulder peak at 240 °C for CuFeO₂-6 represents the reduction of impurity Cu₂O phase to Cu⁰. The peak intensity decreases with increasing synthesis time from 6 to 24 h. Spinel CuFe₂O₄ starts its first reduction of Cu in a lower temperature <250 °C. Reduction of iron in CuFe₂O₄ begins between 400 and 450 °C, which is consistent with the reported reduction temperature of Fe³⁺ to Fe²⁺ [34], and complete reduction to metallic Fe is observed ~650 °C. The final reduction temperature is significantly higher than that of CuFeO₂ (~550 °C) though both catalysts contain reduction promoter Cu. Hence, the reducibility to metallic state is higher for CuFeO₂ than CuFe₂O₄.

Another proposed role of copper is to facilitate the *in-situ* carburization iron to the active carbide phase during the CO₂ hydrogenation. The XRD analysis in Fig. 3b after CO₂ hydrogenation at 300 °C for 16 h indicates that ex-CuFeO₂ catalyst has the doublet peaks at the similar positions of reduced catalysts, but the intensity of Fe peak is greatly reduced and many small new peaks appear, which are identified as diffraction peaks of Hägg iron carbide (χ -Fe₅C₂) as highlighted in the inset. In ex-CuFe₂O₄ catalyst, the intensity of Fe metal peak is reduced, but the formation of the carbide could not be identified. No particular change is observed for the used ex-Fe₂O₃ catalyst after the reaction. Post-reaction XPS analysis in Fig. S8 reveals that both of Fe 2p_{3/2} and 2p_{1/2} spectra appear at 711.0 and 723.5 eV, respectively, for ex-CuFeO₂ and ex-CuFe₂O₄. The peak positions indicate that oxidized Fe species are present on the surface of both catalysts, but that ex-CuFeO₂ is more reduced because of dominant peaks at 710.3 eV, indicating Fe²⁺. On the other hand, a small, lower binding energy of 708 eV is only observed in ex-CuFeO₂, attributable to χ -Fe₅C₂ peak [35] formed during CO₂ hydrogenation. The XPS spectra of C 1p in Fig. S6c and d indicate that ex-CuFeO₂ contains carbonate species and carbon–carbon chains, while ex-CuFe₂O₄ contains only carbonate peaks. Hence, both XRD and XPS indicate the formation of the χ -Fe₅C₂ phase during the reaction only in ex-CuFeO₂ catalyst.

Our attempts to positively identify χ -Fe₅C₂ formation by XRD and XPS were only partly successful because XRD is not that sensitive for the materials of low crystallinity and XPS provides only near-surface information. Hence, X-ray absorption near-edge structure (XANES) spectroscopy was employed, which is an element specific, low concentration-sensitive, crystallinity-independent and local bulk structure-determining probe. Fig. 4a displays the Fe K-edge XANES spectra of delafossite CuFeO₂ catalysts. As-prepared CuFeO₂ has the same edge-rising portion as the reference Fe₂O₃ in terms of energy and shape, denoting a Fe³⁺ state. When reduced with hydrogen, the spectrum is shifted to a lower energy, which is identical to Fe foil. The catalyst after CO₂ hydrogenation at 300 °C for 16 h seems to have a similar edge position to Fe foil, but the edge-rising features are clearly different from each other. Spinel CuFe₂O₄ and hematite Fe₂O₃ catalysts were also analyzed as shown in Fig. 4b and c. In the case of CuFe₂O₄, the edge-rising position in the spectrum of as-prepared sample is close to Fe₂O₃ and CuFeO₂, but the edge feature above 7124 eV is different because CuFeO₂ and CuFe₂O₄ have their unique arrangements of neighboring atoms around a central iron as shown in the structural models in Fig. S9 of SI. The reduced sample exhibits near-edge feature at the lower energy region of 7110–7122 eV, but crossing edge-rising feature is observed at 7123 eV. Unlike CuFeO₂, Fe³⁺ in CuFe₂O₄ is reduced only to Fe^{δ+} rather than Fe⁰. Moreover, the Fe state does not change after the reaction. The Fe₂O₃ catalyst shows close similarity to Fe foil when treated with hydrogen. The used Fe₂O₃ catalyst exhibits distinctly different XANES spectrum as compared to the reduced sample. For more detailed analysis, the derivative spectra of normalized absorbance are compared for all catalysts after the reaction in Fig. 4d. The Fe K-edge XANES spectrum of the used CuFeO₂ catalyst is very similar to that of the reference Hägg iron carbide (χ -Fe₅C₂) prepared by the reported method [36,37]. However, CuFe₂O₄ and Fe₂O₃ exhibit entirely different spectra from that of Hägg iron carbide. The study of Cu K-edge

XANES exhibits the full reduction of Cu⁺ in CuFeO₂ and Cu²⁺ in CuFe₂O₄ to Cu⁰ state, which is maintained during the reaction (Fig. S10).

4. Discussion

Results of H₂-TPR, XRD, XPS and XANES analyses provide a consistent picture of the structural evolution of the catalysts from the precursor state to post-reaction as follows. Compared with Fe₂O₃ and CuFe₂O₄, Fe³⁺ in delafossite CuFeO₂ is reduced to Fe⁰ to the greatest extent in the pre-reduction at 400 °C in H₂. This reduced state seems to play an essential role to form Hägg carbide *in situ* during the CO₂ hydrogenation reaction, which is the known active phase of iron-based catalysts in CO-FT synthesis and appears to be the active phase of CO₂ hydrogenation as well. The presence of copper in the catalyst is important to help Fe³⁺ readily reduced as is well established in CO-FT synthesis over iron-based catalysts [38]. However, we have demonstrated that the nature of precursor is critical in the reduction process. References of Cu₂O-Fe₂O₃ and spinel CuFe₂O₄ show only marginal promotional effects by copper although they also contain copper in separate phases or in a single phase, respectively. The origin of the different reducibility among the different precursors is not obvious. The spinel CuFe₂O₄ is usually synthesized at a high temperature over 800 °C and highly stable in static conditions with both metals in the fully oxidized states of Cu²⁺ and Fe³⁺. But Cu in CuFeO₂ is in the intermediate oxidation state of Cu⁺, and thus it may be thermodynamically less stable against reduction. Kinetically, it was reported that the rate constant at 543 K for the reduction to α-Fe was ca. 3.5 times higher for CuFeO₂ compared to CuFe₂O₄ [39]. Thus, swift reduction and *in-situ* carburization of CuFeO₂ during the reaction forms effectively the Hägg carbide, the known active catalytic phase for FT synthesis. In addition, 0.03% of Na was detected in the ICP analysis of the catalyst. Hence, a synergistic effect between the carbide phase and the small amount of alkali promotor seems responsible for the selective formation of heavier hydrocarbons. Relative to the Fe₂O₃-derived catalyst, the delafossite-derived catalyst shows improved higher hydrocarbon (C₅⁺) selectivity from ~2% to ~65%, and increased olefin to paraffin ratio, whereas methane selectivity is greatly suppressed from ~60% to 2–3%.

5. Conclusions

Delafossite-CuFeO₂ becomes a precursor to Cu–Fe catalysts that produce higher liquid hydrocarbons with a selectivity of ~65%, an olefin-to-paraffin ratio of ~7.3, and minimal methane selectivity of 2–3%. This represents a typical product distribution obtained from FT synthesis from CO over efficient iron-based catalysts. This represents the first demonstration that liquid fuels and olefins of high value and large market could be obtained from CO₂, the most troublesome greenhouse gas. The unique role of delafossite-CuFeO₂ as the catalyst precursor is attributed to the swift reduction and selective carburization to form the Hägg iron carbide (χ -Fe₅C₂), which is the active catalytic phase for the formation of higher hydrocarbons in CO₂ hydrogenation. Other precursors like Cu₂O-Fe₂O₃ and CuFe₂O₄ are not effective in the formation of the active phase although they contain copper. We believe the new catalyst breaks through the limitation of CO₂-based FT synthesis and will open the avenue for new opportunity for recycling CO₂ into valuable fuels and chemicals.

Acknowledgement

This work was supported by Brain Korea Plus Program of Ministry of Education, Korean Center for Artificial Photosynthesis

(NRF-2011-C1AAA0001-2011-0030278), the Basic Science Grant (NRF-2015R1A2A1A10054346), Climate Change Response project (2015M1A2A2074663) funded by MISIP and Project No. 10050509 funded by MOTIE of Republic of Korea.

Appendix A. Supplementary data

Supplementary data associated with this article can be found, in the online version, at <http://dx.doi.org/10.1016/j.apcatb.2016.09.072>.

References

- [1] X.G. Lim, *Nature* 526 (2015) 628–630.
- [2] D. Preti, C. Resta, S. Squarcialupi, G. Fachinetti, *Angew. Chem. Int. Ed.* 50 (2011) 12551–12554.
- [3] N.A.M. Razali, K.T. Lee, S. Bhatia, A.R. Mohamed, *Renew. Sustain. Energy Rev.* 16 (2012) 4951–4964.
- [4] M. He, Y. Sun, B. Han, *Angew. Chem. Int. Ed.* 52 (2013) 9620–9633.
- [5] R.W. Dorner, D.R. Hardy, F.W. Williams, H.D. Willauer, *Energy Environ. Sci.* 3 (2010) 884–890.
- [6] G. Centi, E.A. Quadrelli, S. Perathoner, *Energy Environ. Sci.* 6 (2013) 1711–1731.
- [7] U. Rodemerck, M. Holena, E. Wagner, Q. Smejkal, A. Barkschat, M. Baerns, *ChemCatChem* 5 (2013) 1948–1955.
- [8] S. Perathoner, G. Centi, *ChemSusChem* 7 (2014) 1274–1282.
- [9] M.V. Landau, R. Vidruk, M. Herskowitz, *ChemSusChem* 7 (2014) 785–794.
- [10] S. Saiedi, N.A.S. Amin, M.R. Rahimpour, *J. CO₂ Util.* 5 (2014) 66–81.
- [11] F. MacDonald, *Science Alert*, 27 Apr. 2015, <http://www.sciencealert.com/audi-have-successfully-made-diesel-fuel-from-air-and-water>.
- [12] J. Luo, J.-H. Im, M.T. Mayer, M. Schreier, M.K. Nazeeruddin, N.-G. Park, S.D. Tilley, H.J. Fan, M. Grätzel, *Science* 345 (2014) 1593–1596.
- [13] K. Sivula, R. van de Krol, *Nat. Rev. Mater.* 1 (2016) 15010.
- [14] Y.J. Jang, I. Jeong, J. Lee, J. Lee, M.J. Ko, J.S. Lee, *ACS Nano* 10 (2016) 6980–6987.
- [15] T. Sakakura, J.-C. Choi, H. Yasuda, *Chem. Rev.* 107 (2007) 2365–2387.
- [16] W. Wang, W. Wang, X. Ma, J. Gong, *Chem. Soc. Rev.* 40 (2011) 3703–3727.
- [17] G. Kishan, M.-W. Lee, S.-S. Nam, M.-J. Choi, K.-W. Lee, *Catal. Lett.* 56 (1998) 215–219.
- [18] H. Ando, Y. Matsumura, Y. Souma, *J. Mol. Catal. A* 154 (2000) 23–29.
- [19] L.M. Chew, P. Kangvansura, H. Ruland, H.J. Schulte, C. Somsen, W. Xia, G. Eggerer, A. Worayingyong, M. Muhrer, *Appl. Catal. A* 482 (2014) 163–170.
- [20] F. Ding, A. Zhang, M. Liu, X. Guo, C. Song, *RSC Adv.* 4 (2014) 8930–8938.
- [21] M. Al-Dossary, A.A. Ismail, J.L.G. Fierro, H. Bouzid, *Appl. Catal. B* 165 (2015) 651–660.
- [22] S.R. Yan, K.-W. Jun, J.-S. Hong, M.-J. Choi, K.-W. Lee, *Appl. Catal. A* 194–195 (2000) 63–70.
- [23] S. Li, H. Guo, C. Luo, H. Zhang, L. Xiong, X. Chen, L. Ma, *Catal. Lett.* 143 (2013) 345–355.
- [24] X. Qiu, M. Liu, K. Sunada, M. Miyauchi, K. Hashimoto, *Chem. Commun.* 48 (2012) 7365–7367.
- [25] M.M. Moharam, M.M. Rashad, E.M. Elsayed, R.M. Abou-Shahba, *J. Mater. Sci. Mater. El.* 25 (2014) 1798–1803.
- [26] Y. Dong, C. Cao, Y.-S. Chui, J.A. Zapien, *Chem. Commun.* 50 (2014) 10151–10154.
- [27] A.M. Sukeshini, H. Kobayashi, M. Tabuchi, H. Kageyama, *Solid State Ionics* 128 (2000) 33–41.
- [28] L. Lu, J.-Z. Wang, X.-B. Zhu, X.-W. Gao, H.-K. Liu, *J. Power Sources* 196 (2011) 7025–7029.
- [29] H.M.T. Galvis, C.B. Khare, M. Ruitenbeek, A.I. Dugulan, K.P. de Jong, *Science* 335 (2012) 835–838.
- [30] J.C. Park, D.H. Chun, J.-I. Yang, H.-T. Lee, S. Hong, G.B. Rhim, S. Jang, H. Jung, *RSC Adv.* 5 (2015) 44211–44217.
- [31] E. de Smit, F.M. de Groot, R. Blume, M. Hävecker, A. Knop-Gericke, B.M. Weckhuysen, *Phys. Chem. Chem. Phys.* 12 (2010) 667–680.
- [32] V.R.R. Pendyala, G. Jacobs, M.K. Gnanamani, Y. Hu, A. MacLennan, B.H. Davis, *Appl. Catal. A* 495 (2015) 45–53.
- [33] H.-Y. Lin, Y.-W. Chen, C. Li, *Thermochim. Acta* 400 (2003) 61–67.
- [34] V. Subramanian, E.S. Gnanakumar, D.-W. Jeong, W.-B. Han, C.S. Gopinath, H.-S. Roh, *Chem. Commun.* 49 (2013) 11257–11259.
- [35] K. Cheng, V.V. Ordovsky, M. Virginie, B. Legras, P.A. Chernavskii, V.O. Kazak, C. Cordier, S. Paul, Y. Wang, A.Y. Khodakov, *Appl. Catal. A* 488 (2014) 66–77.
- [36] C. Yang, H. Zhao, Y. Hou, D. Ma, *J. Am. Chem. Soc.* 134 (2012) 15814–15821.
- [37] H. Park, D.H. Youn, J.Y. Kim, W.Y. Kim, Y.H. Choi, Y.H. Lee, S.H. Choi, J.S. Lee, *ChemCatChem* 7 (2015) 3488–3494.
- [38] J.W. Bae, S.-J. Park, S.-H. Kang, Y.-J. Lee, K.-W. Jun, Y.-W. Rhee, *J. Ind. Eng. Chem.* 15 (2009) 798–802.
- [39] Z.H. Chonco, A. Ferreira, L. Lodya, M. Claeys, E. van Steen, *J. Catal.* 307 (2013) 283–294.